nature genetics

Genetic lineage tracing identifies endocardial origin of liver vasculature

Hui Zhang[1], Wenjuan Pu[1], Xueying Tian[1], Xiuzhen Huang[1], Lingjuan He[1], Qiaozhen Liu[1], Yan Li[1], Libo Zhang[1], Liang He[1], Kuo Liu[1,2], Astrid Gillich[3] & Bin Zhou[1,2,4]

The hepatic vasculature is essential for liver development, homeostasis and regeneration, yet the developmental program of hepatic vessel formation and the embryonic origin of the liver vasculature remain unknown. Here we show in mouse that endocardial cells form a primitive vascular plexus surrounding the liver bud and subsequently contribute to a substantial portion of the liver vasculature. Using intersectional genetics, we demonstrate that the endocardium of the sinus venosus is a source for the hepatic plexus. Inhibition of endocardial angiogenesis results in reduced endocardial contribution to the liver vasculature and defects in liver organogenesis. We conclude that a substantial portion of liver vessels derives from the endocardium and shares a common developmental origin with coronary arteries.

Blood vessels are essential for liver function, homeostasis and regeneration upon injury[1]. Reduced blood supply, or liver ischemia, causes impairment of organ function and can result in liver failure[2]. Determining the developmental program of hepatic vessel formation could provide a foundation for the design of strategies to stimulate vessel growth upon liver regeneration[3,4]. During embryonic development, blood vessels not only form passive conduits to deliver oxygen and nutrients, but they also establish instructive developmental niches to promote liver organogenesis before the onset of circulation in mouse embryos[5]. Reciprocal signaling between the endothelium and endoderm during early development directs the stepwise differentiation and morphogenesis program required for organogenesis[5–7]. The liver vasculature also constitutes the cellular basis of the hematopoietic stem cell niche in late embryonic and neonatal stages, promoting hematopoietic stem cell expansion before migration to the bone marrow[8]. In the mature organ, the liver vasculature provides an instructive niche that mediates hepatic regeneration[1,3,4]. In spite of the important functions of the liver vasculature during development, homeostasis and regeneration, its developmental origin remains unknown[2]. In the present study, we performed lineage tracing in mice to determine the developmental origin of hepatic vessels. We find that a substantial number of liver vascular endothelial cells arise from the dorsal part of the endocardium. Our studies also indicate that the developing endocardium regulates liver organogenesis through vascular endothelial cell contribution.

RESULTS

NFATC1 marks developing endocardium but not liver vasculature

In the heart, the developmental origin for coronary arteries has been a focus of intensive debate[9–14]. As part of our study on coronary artery origin, we performed lineage tracing in mice of the endocardium. We found an unexpected contribution of NFATC1$^+$ endocardial cells to the primitive hepatic plexus. In mice, the early cardiac tube forms by fusion of the cardiac crescent at the midline and then undergoes looping at embryonic day (E) 8.0 to E8.5 (ref. 15). Whole-mount immunostaining of E8.0 and E8.5 embryos for cardiac troponin I type 3 (TNNI3) showed that the looping heart is composed of ventricle, atrium and sinus venosus (SV) compartments, all of which express TNNI3 (**Supplementary Fig. 1a**,**b**). Co-staining for TNNI3 and the pan-endothelial marker PECAM1 on sections from E8.0 and E8.5 embryos showed that PECAM1$^+$ endocardium is surrounded by TNNI3$^+$ cardiomyocytes (**Supplementary Fig. 1c–e**). The two SV horns are located at the caudal part of the developing heart and reside on the flanks of the foregut diverticulum (**Supplementary Fig. 1c–e**). These data demonstrate that the atrium and SV horns reside close to the foregut endoderm in the developing embryo.

Cardiac endocardial cells represent a unique population of endothelial cells that express NFATC1 during development[16–18]. We generated a tamoxifen-inducible *Nfatc1*-IRES-*creER* knock-in line (**Fig. 1a**) and first analyzed expression of estrogen receptor (ESR) as a surrogate for NFATC1 expression. Whole-mount immunostaining showed that ESR was expressed in the developing heart of *Nfatc1*-IRES-*creER* embryos at E7.75–E9.0 (**Fig. 1b**). Co-staining of ESR and either TNNI3 or NKX2-5 as a cardiac marker confirmed that ESR expression was restricted to the cardiac region (**Fig. 1c**). Immunostaining for ESR on sections from E8.5 *Nfatc1*-IRES-*creER* embryos showed ESR expression in atrial, ventricular and SV endocardium (**Fig. 1d**). Co-staining of endoglin (ENG) and ESR showed ESR expression in endocardium (**Fig. 1e**). By examining

[1]Key Laboratory of Nutrition and Metabolism, Institute for Nutritional Sciences, Shanghai Institutes for Biological Sciences, Graduate School of the Chinese Academy of Sciences, Chinese Academy of Sciences, Shanghai, China. [2]School of Life Science and Technology, ShanghaiTech University, Shanghai, China. [3]Department of Biochemistry, Stanford University School of Medicine, Stanford, California, USA. [4]Institute of Neuroscience, State Key Laboratory of Neuroscience, Chinese Academy of Sciences Center for Excellence in Brain Science and Intelligence Technology, Shanghai Institutes for Biological Sciences, Chinese Academy of Sciences, Shanghai, China. Correspondence should be addressed to B.Z. (zhoubin@sibs.ac.cn).

Received 6 January; accepted 4 March; published online 28 March 2016; doi:10.1038/ng.3536

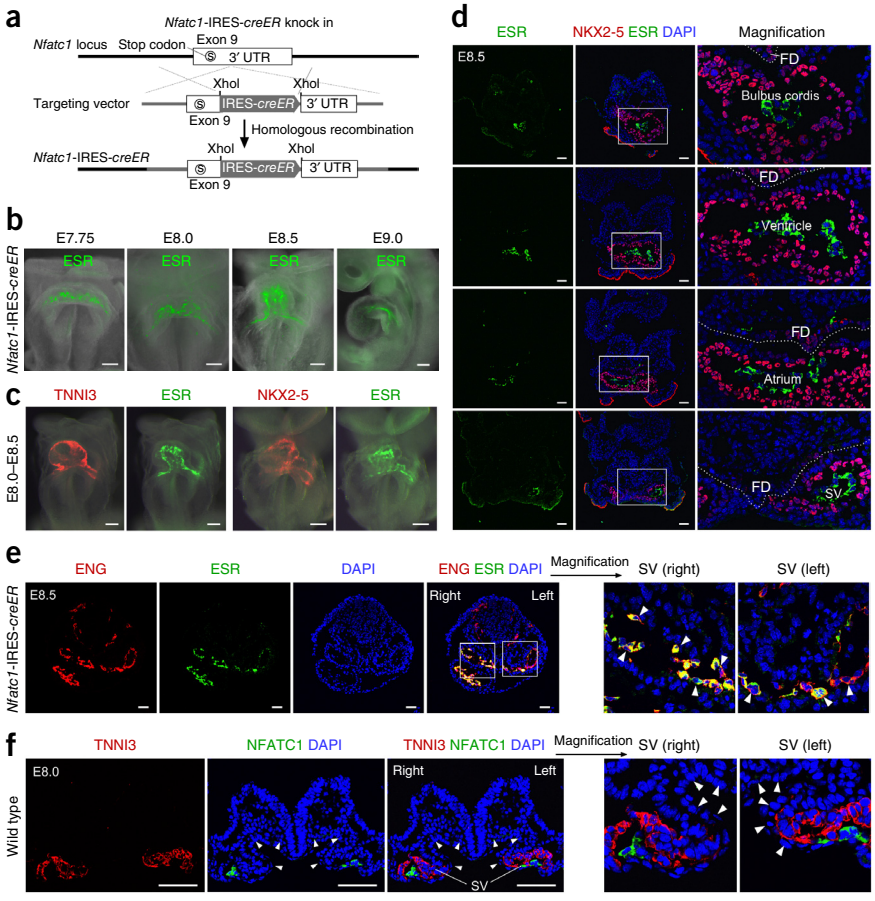

Figure 1 NFATC1 is expressed in the endocardium of the atrium, ventricle and sinus venosus. (**a**) Schematic showing the strategy for generation of the *Nfatc1*-IRES-*creER* knock-in line by homologous recombination. (**b**) Whole-mount staining for estrogen receptor (ESR) on E7.75–E9.0 *Nfatc1*-IRES-*creER* embryos. (**c**) Whole-mount view of E8.0–E8.5 embryos stained for ESR and the cardiac marker NKX2-5 or TNNI3. (**d**) Immunostaining for NKX2-5 and ESR on E8.5 *Nfatc1*-IRES-*creER* embryonic sections. Dotted lines indicate foregut diverticulum (FD); SV, sinus venosus. Right panels are magnified views of the boxed regions in middle panels. (**e**) Immunostaining for endoglin (ENG) and ESR on E8.5 *Nfatc1*-IRES-*creER* embryonic section shows ESR (NFATC1) expression (arrowheads) in the endocardium of the right and left SV horns (boxed regions). (**f**) Immunostaining for TNNI3 and NFATC1 on E8.0 wild-type embryonic sections shows NFATC1 expression in the right and left SV horns but not in foregut diverticulum (arrowheads). Scale bars, 100 μm. Each image is representative of three individual samples.

consecutive sections of *Nfatc1*-IRES-*creER* whole embryos, we found that ESR was specifically expressed in the atrial, ventricular and SV endocardium of the early developing heart (**Supplementary Fig. 2**).

To assess the proximity of caudal endocardium to hepatic endoderm, we generated *Nfatc1-GFP* reporter mice and stained *Nfatc1-GFP* embryos for molecular markers of the foregut and hepatic endoderm, including FOXA2 for detection of foregut endoderm before E9.0 and HNF4A for detection of hepatic endoderm after E9.0. Immunostaining of *Nfatc1-GFP* embryos for GFP and FOXA2 or HNF4A showed that the caudal part of the NFATC1$^+$ endocardium was located on the flanks of the FOXA2$^+$ foregut diverticulum at E8.0 and E8.5 (**Supplementary Fig. 3a**,**b**). GFP expression was not detected in the liver bud or SV from E9.5 to E11.5 (**Supplementary Fig. 3c**). Yet, the SV marked by vascular endothelial cadherin (CDH5 or VE-cadherin) was located in close proximity to the HNF4A$^+$ liver bud at E9.5 and E10.5, forming a continuum with the hepatic vasculature (**Supplementary Fig. 3c**).

To further validate the expression of NFATC1, we performed immunostaining for NFATC1 on embryonic sections. NFATC1 was expressed in the endocardium of the SV horns at E8.0 (**Fig. 1f**), but its levels were reduced in SV endocardium at E9.5 (**Supplementary Fig. 4a**). Immunostaining for NFATC1 and ESR or GFP on *Nfatc1*-IRES-*creER* and *Nfatc1-GFP* embryonic sections, respectively, showed that at E9.5 ESR or GFP was colocalized with NFATC1, which was not detected in SV endocardium or liver bud (**Supplementary Fig. 4b**). Around E10.5, hematopoietic stem cells started to colonize the fetal liver, which serves as a major hematopoietic organ after E11.5 in mouse embryos[19,20]. We could detect NFATC1 in a subset of these hematopoietic cells but not in liver endothelial cells or SV endocardium at E10.5 and E11.5 (**Supplementary Fig. 4c**,**d**). There were no NFATC1$^+$ endothelial cells in the liver at E12.5, E13.5 or E15.5 (**Supplementary Fig. 4e**–**g**). Similarly, there were no ESR$^+$ or GFP$^+$ endothelial cells in *Nfatc1*-IRES-*creER* and *Nfatc1-GFP* embryonic livers, respectively, at E12.5, E13.5 or E15.5 (**Supplementary Fig. 5a**,**b**). Taken together, the above data demonstrate that NFATC1 and the NFATC1 surrogates ESR and GFP are not expressed in liver vascular endothelial cells.

NFATC1$^+$ endocardial cells contribute to liver vasculature

Recent studies reported a contribution of ventricular and SV endocardium to the coronary vasculature in mice[10–12]. Because we found that the caudal part of the endocardium is located in proximity to the foregut endoderm and liver bud at times of hepatic vessel formation, we investigated whether the endocardium forms liver vasculature in addition to coronary arteries. To lineage trace the developing endocardium, we first crossed *Nfatc1-dre* mice with the *rox* reporter line *Rosa26-rox*-STOP-*rox-RFP* (*Rosa26*-RSR-*RFP*) to generate *Nfatc1-dre*; *Rosa26*-RSR-*RFP* embryos[21]. Dre, like Cre, is a site-specific recombinase and targets *rox* sites for recombination; it has previously been used for lineage tracing[22–24]. In our embryos, Dre-mediated recombination leads to irreversible removal of the *rox*-flanked stop cassette and permanent labeling of cells, including NFATC1$^+$ cells and their descendants, with RFP (**Fig. 2a**). We found that *Nfatc1*-driven Dre expression led to RFP labeling of atrial, ventricular and SV endocardium at E8.5, E9.0 and E9.5 (**Fig. 2b**–**d**). Although NFATC1 was not expressed in the primitive vasculature of the liver bud (**Supplementary Figs. 3c**, **4c**–**g** and **5a**,**b**), we found descendants of NFATC1$^+$ cells surrounding the hepatic endoderm at E9.0 and in the liver vasculature at E9.5 and E10.5 (**Fig. 2c**–**e**). Analysis of livers collected from *Nfatc1-dre*; *Rosa26*-RSR-*RFP* embryos at E13.5 and E15.5 showed that a substantial portion of the liver vasculature (~40%) was labeled with RFP (**Fig. 2f**–**h**), indicating that NFATC1$^+$ endocardial cells contribute to liver vessels. We did not detect RFP labeling of hepatocytes, stellate cells, smooth muscle cells, cholangiocytes,

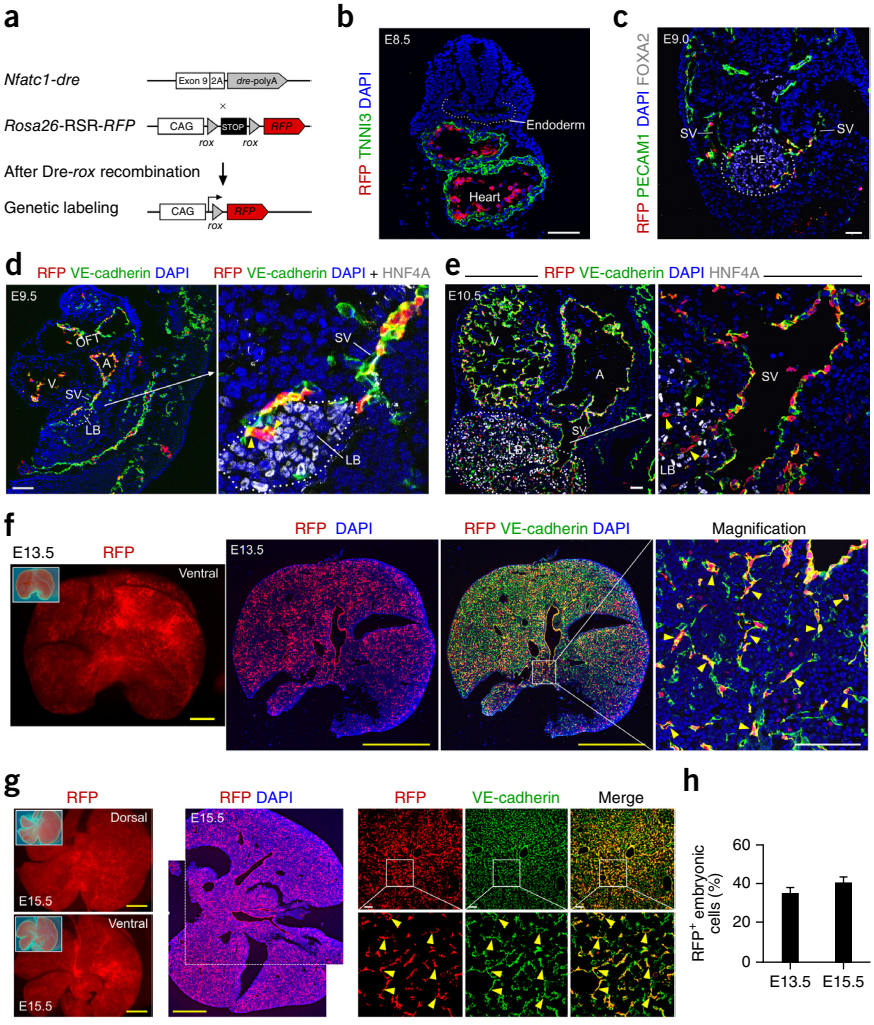

Figure 2 NFATC1$^+$ endocardial cells contribute to vessels in the developing liver. (**a**) Strategy of genetic lineage tracing based on Dre-mediated recombination at *rox* sites using *Nfatc1-dre* and *Rosa26*-RSR-*RFP* reporter lines. (**b**) Immunostaining for RFP and TNNI3 on E8.5 *Nfatc1-dre*; *Rosa26*-RSR-*RFP* embryonic sections. RFP expression is restricted to cardiac endocardium, with no detectable expression in endoderm (dotted line). (**c**–**e**) Immunostaining for RFP, VE-cadherin or PECAM1, and FOXA2 or HNF4A on sections of E9.0 (**c**), E9.5 (**d**) and E10.5 (**e**) *Nfatc1-dre*; *Rosa26*-RSR-*RFP* embryos. The dotted lines indicate hepatic endoderm (HE; E9.0) and liver bud (LB; E9.5 and E10.5). Hepatic endothelial cells are labeled with RFP (arrowheads). The arrow indicates the magnified view of the region in the left panel. (**f**,**g**) Whole-mount and section views of E13.5 (**f**) and E15.5 (**g**) livers. Immunostaining for RFP and VE-cadherin shows the contribution of lineage-labeled cells to liver endothelial cells (arrowheads). Magnified views of the boxed regions are shown in the far right panels. (**h**) Quantification of lineage labeling in E13.5 and E15.5 liver endothelium. $n = 4$. Error bars, s.e.m. A, atrium; V, ventricle; OFT, outflow tract. Scale bars: yellow, 1 mm; white, 100 μm.

biliary epithelial cells or fibroblasts in the liver (**Supplementary Fig. 6**).

We next aimed to test whether NFATC1$^+$ endocardial cells contribute to the liver vasculature by inducible genetic lineage tracing using *Nfatc1*-IRES-*creER* embryos (**Fig. 3b**). Immunostaining for ESR, FOXA2 and PECAM1 showed that CreER$^+$ SV is in close contact with foregut diverticulum at E8.0 and hepatic endoderm at E8.5 and E9.0 (**Fig. 3a**). Similarly to NFATC1 expression (**Supplementary Fig. 4a**–**d**) and also GFP expression in *Nfatc1-GFP* embryos (**Supplementary Fig. 3c**), CreER expression was markedly reduced in SV at E9.0 and could hardly be detected in SV or liver bud at E9.5–E14.5 (**Fig. 3a** and **Supplementary Fig. 7a**,**b**). To test whether NFATC1$^+$ endocardial cells contribute to liver vessels, we injected tamoxifen into *Nfatc1*-IRES-*creER* mice crossed to mice with a stop cassette flanked by *loxP* sites upstream of *RFP* at the *Rosa26* locus (*Rosa26-loxP*-STOP-*loxP-RFP*, or *Rosa26-RFP*) at E8.0 and analyzed the extent of labeling with RFP at E9.5–E14.5 (**Fig. 3b**). In these mice, tamoxifen administration leads to nuclear translocation of CreER^{T2} in NFATC1$^+$ cells, which removes the stop cassette and leads to RFP expression. Thus, CreER$^+$ cells and their descendants are permanently labeled by the tracing marker RFP. We detected labeling in atrial, ventricular and SV endocardium, as well as the primitive vasculature in the liver bud (**Supplementary Fig. 7c**,**d**). By immunostaining for RFP and VE-cadherin, we found RFP$^+$ endothelial cells in the liver but not in lung, stomach or intestine (**Fig. 3c**,**d**), indicating that NFATC1$^+$ endocardial cells give rise to liver vessels during embryonic development. Quantification of the RFP$^+$VE-cadherin$^+$ endothelial cells in E12.5–E14.5 livers showed that inducible CreER labeled 39.12 ± 5.05% of endothelial cells. Given that NFATC1 is not expressed in SV endocardium at E9.5 and afterward, tamoxifen administration at E9.5 resulted in abrogated genetic labeling of endothelial cells in E13.5 liver, whereas endocardium in the ventricle was still labeled (**Fig. 3e**–**g**). Taken together, the above data suggest that SV endocardial cells contribute to the fetal liver vasculature between E8 and E9.

Sinus venosus is the main endocardial source for liver vasculature

SV endocardium is a major source for coronary vasculature in the developing heart[10,25]. At E8.5–E10.5, atrial and SV endocardium were closer to hepatic endoderm than ventricular endocardium (**Fig. 3a** and **Supplementary Fig. 7**). We therefore hypothesized that the caudal part of the endocardium, either atrium or SV, gives rise to the liver vasculature. To address this hypothesis, we targeted the endocardial gene *Npr3*, which encodes natriuretic peptide receptor 3, and generated *Npr3-creER* knock-in mice for lineage tracing. Whole-mount immunostaining for ESR showed CreER expression in atrial and ventricular endocardium but not in SV (**Supplementary Fig. 8a**). This expression pattern was confirmed by *in situ* hybridization for *Npr3* (**Supplementary Fig. 8b**). Immunostaining for ESR, PECAM1 or VE-cadherin, and FOXA2 or HNF4A showed CreER expression in atrial and ventricular endocardium but not in SV or hepatic endoderm from E8.5 to E10.5 (**Supplementary Fig. 8c**–**f**). Tamoxifen injection of *Npr3-creER*; *Rosa26-RFP* mice at E8.0 did not result in labeling of SV nor liver vasculature at E10.5 and E11.5 (**Supplementary Fig. 9a**–**c**). Liver labeling was negligible at E13.5, whereas the heart from the same embryo was strongly labeled (**Supplementary Fig. 9d**). Immunostaining of RFP and VE-cadherin on liver and heart sections from the same embryo showed labeling of ventricular endocardium

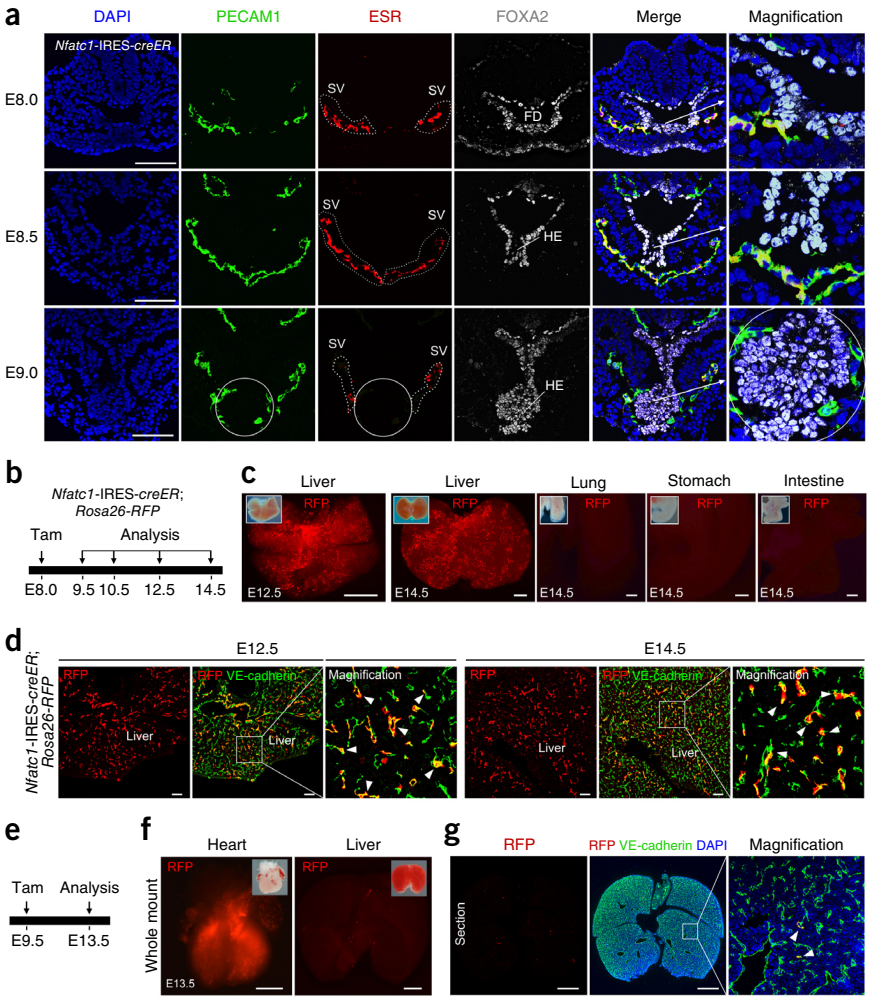

Figure 3 *Nfatc1*-IRES-*creER* embryos have labeling of SV endocardium and liver vasculature. (**a**) Immunostaining for FOXA2, ESR and PECAM1 on sections from *Nfatc1*-IRES-*creER* embryos. A subset of endocardial cells in the left and right SV horns (dotted lines) surround the foregut diverticulum and hepatic endoderm. Arrows indicate magnified views of the regions in the merged images. Circled regions are hepatic endoderm. (**b**) Strategy of labeling using the *Nfatc1*-IRES-*creER* and *Rosa26-RFP* reporter lines. Tamoxifen (Tam) was injected at E8.0, and labeling was analyzed at later stages (E9.5–E14.5). (**c**) Whole-mount views of E12.5 and E14.5 livers from *Nfatc1*-IRES-*creER*; *Rosa26-RFP* embryos. Insets are bright-field images. (**d**) Immunostaining for RFP and VE-cadherin on embryonic liver sections showing labeling of VE-cadherin$^+$ cells by RFP (arrowheads). Magnified views of the boxed regions are shown to the right. (**e**) Schematic showing tamoxifen treatment and analysis. (**f**) Whole-mount views of heart and liver from the same embryo. (**g**) Immunostaining for RFP and VE-cadherin on liver sections from E13.5 embryos treated with tamoxifen at E9.5. The white arrowheads indicate RFP$^+$VE-cadherin$^+$ vessels. A magnified view of the boxed region is shown to the right. Each image is representative of three individual samples at each stage. Scale bars: 0.5 mm in **c**, **f** and **g**, 100 μm in **a** and **d**.

but not liver vasculature (**Supplementary Fig. 9e**,**f**). Quantification of RFP$^+$ vessels showed that *Npr3-creER* labeled only 0.23 ± 0.14% of endothelial cells in the liver (n = 4). These data demonstrate that *Npr3-creER* labels atrial and ventricular endocardium but not SV endocardium or liver vasculature.

To determine whether SV is the endocardial source for liver vasculature, we compared the fate map of labeled and unlabeled SV endocardium using two strategies. Strategy 1 used *Nfatc1-dre*; *Rosa26*-RSR-*RFP* to label atrial, ventricular and SV endocardium as described (**Fig. 2a**–**e**). Strategy 2 employed *Nfatc1-dre*; *Npr3-creER*; *Rosa26*-RSR-LSL-*RFP* (Ai66) to subtract SV labeling. In this strategy, two recombination events by the Dre and CreER recombinases are required for RFP expression (**Supplementary Fig. 10**). Because *Npr3-creER* labels the endocardium of the atrium and ventricle but not SV (**Supplementary Fig. 9b**,**c**), *Nfatc1-dre*–mediated recombination alone in the Ai66 reporter does not result in SV labeling (**Supplementary Fig. 10**). We employed this approach to address whether SV labeling in cells derived from NFATC1$^+$ cells accounts for labeling of the liver vasculature. Whole-mount fluorescence views of E10.5 embryos showed no RFP expression in SV or liver in strategy 2 but labeling of both regions in strategy 1 (**Fig. 4a**). Immunostaining for RFP, HNF4A and PECAM1 showed that SV endocardium was not labeled in strategy 2, whereas both atrial and ventricular endocardium were labeled in both strategies (**Fig. 4b**). Likewise, whole-mount views and sectional immunostaining showed that E13.5 liver vasculature was not labeled in strategy 2, whereas atrial and ventricular endocardium was labeled in both strategies (**Fig. 4c**,**d**). Quantification of labeled endothelial cells showed a significantly reduced percentage of RFP$^+$ vessels in strategy 2 as compared with strategy 1 (0.19 ± 0.11% versus 37.88 ± 4.05%, $P < 0.05$; $n = 4$). These data demonstrate that liver vasculature is derived from NFATC1$^+$ SV endocardium but not from atrial or ventricular endocardium (**Fig. 4e**).

Inhibition of endocardial angiogenesis impairs liver organogenesis

Reciprocal signaling between endoderm cells and mesoderm-derived endothelial cells directs the stepwise cell differentiation and morphogenesis process during organ development[6,7]. Endothelial cell precursors differentiate into blood vessels in response to angiogenic signals from adjacent tissues[26]. Among these, VEGF family members represent the most potent proangiogenic factors controlling liver organogenesis[5]. We found by *in situ* hybridization that *Vegfa* was highly expressed in the liver bud (**Supplementary Fig. 11a**). VEGFA induces angiogenesis by signaling through VEGF receptor 2 (KDR or VEGFR2, also known as FLK1)[27,28], which has an essential role in vascular development[29,30]. Immunostaining for VEGFR2 and PECAM1 showed that VEGFR2 was expressed in SV endocardium from E8.5–E9.5 (**Supplementary Fig. 11b**,**c**).

These expression patterns suggested that the VEGFA secreted by liver endoderm induces recruitment of VEGFR2$^+$ endocardial cells through angiogenic sprouting[5]. We therefore specifically deleted *Kdr* in the endocardium by crossing *Nfatc1*-IRES-*creER* mice with mice with two *loxP*-flanked alleles of *Kdr* (*Kdr*$^{fl/fl}$; ref. 31) and *Rosa26-RFP* (**Fig. 5a**). Tamoxifen administration leads to translocation of CreER^{T2} into the nucleus and recombination between *loxP* sites, resulting in endocardial deletion of *Kdr* (**Fig. 5b**). We initiated tamoxifen

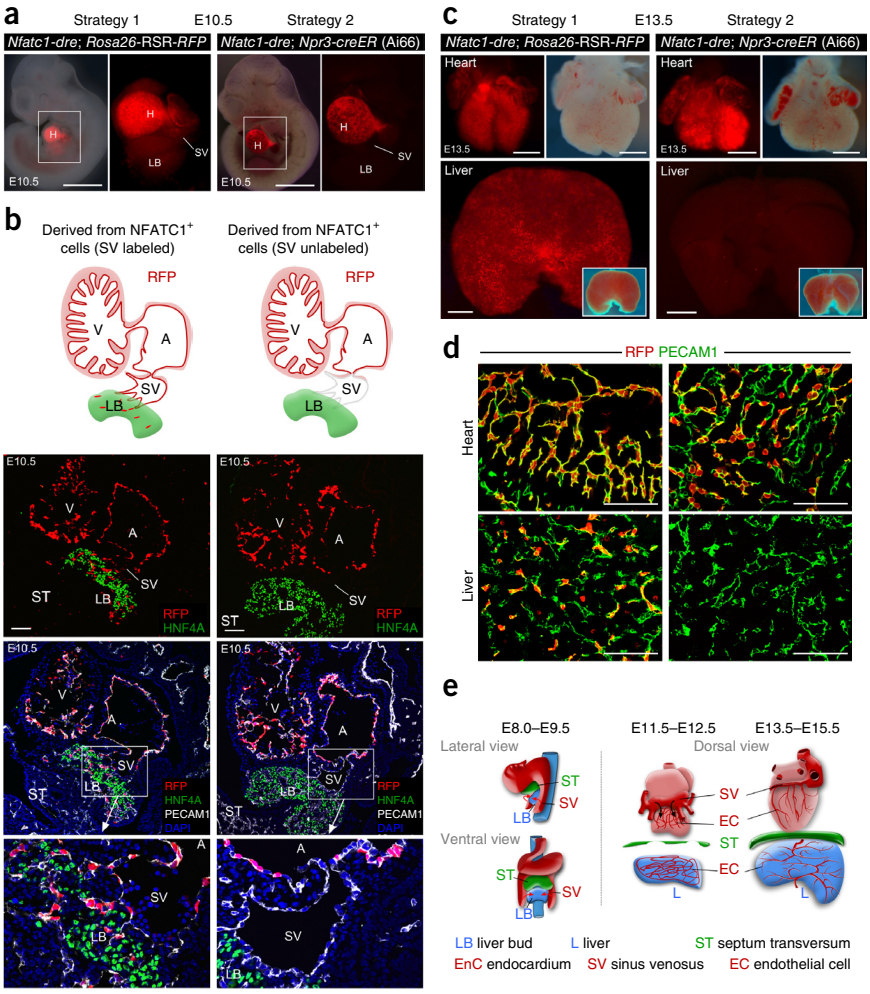

Figure 4 Sinus venosus endocardium contributes to liver vasculature. (**a**) Whole-mount views of E10.5 embryos from lineage tracing strategy 1 (*Nfatc1-dre*; *Rosa26*-RSR-*RFP*) and strategy 2 (*Nfatc1-dre*; *Npr3-creER*; Ai66). SV is labeled by *Nfatc1-dre* in strategy 1 but not by *Nfatc1-dre* in strategy 2. Tamoxifen was injected at E8 for both strategies. H, heart. Magnified views of the boxed regions are shown to the right. (**b**) Immunostaining for RFP, HNF4A and PECAM1 on E10.5 embryonic sections. Liver vasculature and SV are labeled by *Nfatc1-dre* in strategy 1 but not by *Nfatc1-dre* in strategy 2. Insets are bright-field images. (**c**) Whole-mount views of E13.5 hearts and livers from strategies 1 and 2. (**d**) Immunostaining for RFP and PECAM1 on heart and liver sections from strategies 1 and 2. (**e**) Schematic showing the proximity of the developing caudal endocardium to the liver bud and the contribution of SV endocardium to the primitive liver vasculature at E8.0–E9.5. With SV withdrawal to the chest and diaphragm formation, SV endocardium contributes to coronary vessels. Scale bars: 1 mm in **a**, 100 μm in **b** and **d**, 0.5 mm in **c**.

treatment at E8.0–E8.5 and collected *Nfatc1*-IRES-*creER*; *Kdr*$^{fl/fl}$; *Rosa26-RFP* (mutant) and *Nfatc1*-IRES-*creER*; *Kdr*$^{fl/+}$; *Rosa26-RFP* (control) embryos for analysis at E9.5–E13.5 (**Fig. 5a**). Immunostaining for VEGFR2 and VE-cadherin on sections from E9.5 mutant and control embryos showed that VEGFR2 expression was notably lower in endocardium but not in dorsal vessels (**Fig. 5c**). For lineage tracing of endocardial cells, we performed immunostaining for RFP, HNF4A and VE-cadherin on E11.5 embryonic sections and found significantly fewer RFP$^+$ endothelial cells in the liver buds of mutants as compared to controls (**Fig. 5d**). Immunostaining for the hepatocyte marker HNF4A showed liver dysplasia in mutants (**Fig. 5d**). Although the size of the heart was only slightly smaller in mutants at E13.5, the size of the mutant liver from the same embryo was significantly smaller than that of the control embryo (**Fig. 5e**). Quantification of liver volume showed that the size of mutant livers was only about one-quarter that of control livers (**Fig. 5f**), indicating that endocardial *Kdr* deletion impairs liver organogenesis. Immunostaining for RFP and VE-cadherin on E13.5 liver sections showed significantly fewer RFP$^+$ endothelial cells in mutant livers than in control livers ($P < 0.05$; **Fig. 5g**). Quantification data confirmed that the endocardial contribution to liver vasculature was significantly lower in mutants than in controls (**Fig. 5h**). Taken together, these data indicate that the endocardial contribution to liver vasculature is controlled by VEGF signaling, which determines vessel formation and liver organogenesis.

Endocardium-derived liver vessels persist in the adult liver

In the embryonic liver, endocardium-derived cells formed liver endothelial cells in both the portal and central veins (**Supplementary Fig. 12a**). To address whether these endocardium-derived vessels persist in the mature organ, we collected *Nfatc1*-IRES-*creER*; *Rosa26-RFP* adult livers for analysis. Immunostaining for RFP, VE-cadherin and the portal cholangiocyte marker CK19 (KRT19) showed that the endocardium-derived endothelial cells (RFP$^+$VE-cadherin$^+$) resided in portal veins and arteries, sinusoids and central veins (**Supplementary Fig. 12b**). By immunostaining for smooth muscle actin (ACTA2 or SMA) and the venous endothelial cell marker Eph receptor B4 (EPHB4), we confirmed the existence of RFP$^+$ endothelial cells in both portal arteries and veins (**Supplementary Fig. 12c**). Additionally, these RFP$^+$ cells also remained as PROX1$^+$LYVE1$^+$ lymphatic endothelial cells in the adult liver (**Supplementary Fig. 12d**). These data suggest that endocardium-derived embryonic liver vasculature persists and forms multiple types of endothelial cells in the adult liver.

We next asked whether these endocardium-derived vessels respond to liver injury and give rise to new blood vessels during liver regeneration. We performed partial hepatectomy on *Nfatc1*-IRES-*creER*; *Rosa26-RFP* mice and collected livers at 3 or 9 d after injury (**Supplementary Fig. 13a**). Immunostaining for Ki-67, phosphorylated histone H3 (PHH3) and proliferating cell nuclear antigen (PCNA) as proliferation markers on liver sections from the sham and partial hepatectomy groups showed a significant increase in RFP$^+$ endothelial cells during regeneration (**Supplementary Fig. 13b–e**), indicating formation of new blood vessels from endocardium-derived cells in the mature organ. Taken together, these data suggest that endocardium-derived liver endothelial cells respond to injury and proliferate to form new vessels during liver regeneration.

DISCUSSION

Liver development is orchestrated in a stepwise manner by signaling from the cardiac mesoderm and subsequent signals from endothelial cells[7]. The septum transversum has been suggested to contain endothelial cell precursors that contribute to liver vasculature during development[5]. Notably, a recent study suggested that FOXA2$^+$

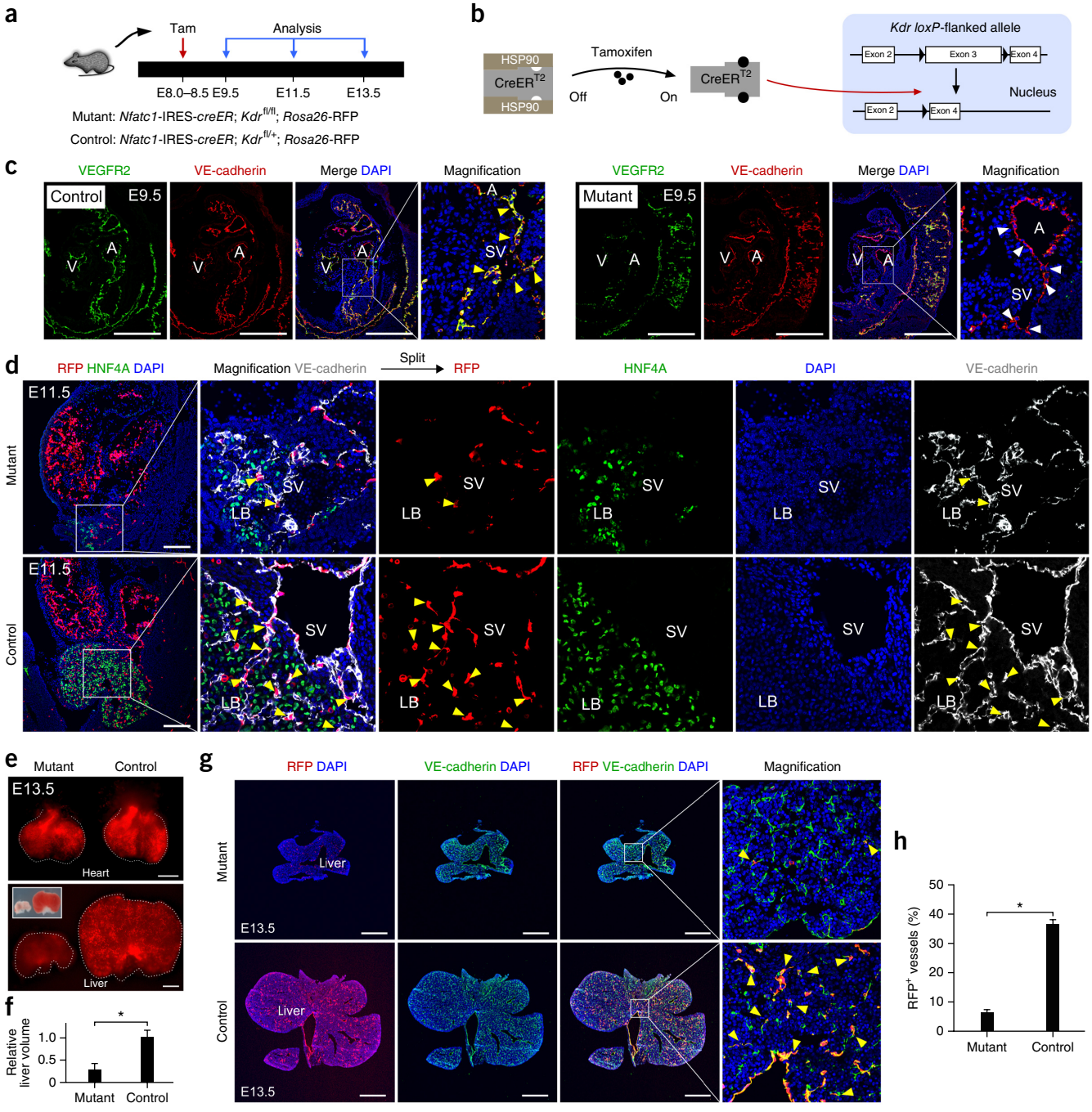

Figure 5 Endocardial deletion of *Kdr* (*Vegfr2*) impairs liver organogenesis. (**a**) Schematic showing the experimental strategy for conditional *Kdr* deletion in endocardial cells. (**b**) Schematic showing the strategy for inducible *Kdr* deletion in endocardial cells. Tamoxifen administration leads to translocation of CreER^{T2} into the nucleus and recombination between *loxP* sites, resulting in deletion of *Kdr* (exon 3) in NFATC1$^+$ endocardial cells. (**c**) Immunostaining for VEGFR2 and VE-cadherin on E9.5 mutant or control embryonic sections. VEGFR2 is readily detected in endocardial cells (yellow arrowheads) from controls but is hardly detected in endocardial cells (white arrowheads) from mutants. (**d**) Immunostaining for RFP, HNF4A and VE-cadherin on E11.5 embryonic sections showing lower numbers of RFP$^+$VE-cadherin$^+$ endothelial cells (arrowheads) in the liver bud of mutants than in controls. (**e**) Whole-mount views of hearts and livers from the same mutant or control embryos. The inset shows bright-field images of liver. (**f**) Quantification of liver volume in mutant and control embryos. Control liver volume was set to 1.0; values are shown as means ± s.e.m. ($n = 4$). Student's *t* test was used to determine statistical significance: $^*P < 0.05$. (**g**) Immunostaining for RFP and VE-cadherin on liver sections from E13.5 mutant and control embryos. Yellow arrowheads indicate RFP$^+$ vessels. (**h**) Quantification of the percentage of RFP$^+$ liver vessels. $^*P < 0.05$; $n = 4$. Error bars, s.e.m. Magnified views of the boxed region are shown to the right in **c**, **d** and **g**. Scale bars: 100 μm in **c** and **d**, 500 μm in **e** and **g**.

endoderm also contributes to a subset of liver endothelial cells during development[32]. Our present work shows that liver vessels arise from the endocardium that constitutes the innermost layer of the developing heart. These hepatic endothelial cells from diverse origins provide a source of signals during liver organogenesis[5], which is reminiscent of the scenario for other endodermal organs such as the pancreas, where blood vessels not only provide metabolic sustenance but also inductive signals for organogenesis[6]. Our finding that inhibition of endocardial angiogenesis impairs liver organogenesis suggests that endocardium-derived cells provide inductive cues for liver development. Thus, our study provides new evidence that a component of one organ (endocardium) influences the development of another organ (liver) through direct vascular contribution. Our work links the origin of endothelial cells and their role in instructive signaling to shape endoderm organogenesis[5,6] during early embryonic development.

This study shows that, during early development, the caudal part of the endocardium is in close proximity to hepatic endoderm and contributes a substantial portion of the primitive vasculature in the liver (**Fig. 4e**). With development of the heart and diaphragm, the SV translocates from the caudal to the cranial side of the heart, withdraws to the chest and is separated from the liver (**Fig. 4e**). A detailed characterization of the lineage potential and heterogeneity of endocardial cells during development, as well as their properties and behavior upon injury, should now be a priority. Unraveling the program of lineage conversion from endocardium to liver vasculature may provide new avenues for therapeutic strategies to stimulate revascularization upon liver regeneration[1,3]. Elucidation of the signals that instruct the endocardium to form liver vasculature or coronary arteries will also highlight similarities and differences in the program of vessel formation and growth in different organs, which merits further investigation in future studies.

METHODS

Methods and any associated references are available in the online version of the paper.

Note: Any Supplementary Information and Source Data files are available in the online version of the paper.

ACKNOWLEDGMENTS

We thank A. Nagy (Mount Sinai Hospital and Samuel Lunenfeld Research Institute) and J. Rossant (Hospital for Sick Children, University of Toronto) for sharing the Kdrfl mouse line and H. Zeng (Allen Institute) for sharing the Ai66 mouse line. We also thank Shanghai Biomodel Organism Co., Ltd., for mouse generation. This work was supported the Ministry of Science and Technology of China (2012CB945102 and 2013CB945302), the National Science Foundation of China (91339104, 31271552, 31222038, 31301188, 31571503 and 31501172), the Shanghai Basic Research Key Project (14JC1407400), the Major Program of Development Fund for the Shanghai Zhangjiang National Innovation Demonstration Zone (ZJ2014-ZD-002 and 2014-2016), the Shanghai Institutes for Biological Sciences (SIBS) President Fund, the Sanofi-SIBS Fellowship, the SIBS Postdoctoral Fund, AstraZeneca, the China Postdoctoral Science Foundation (2015M570389 and 2015M581669), the Youth Innovation Promotion Association of the Chinese Academy of Sciences (2015218), the Shanghai Yangfan Project (15YF1414000) and the Shanghai Rising Star Program (15QA1404300).

AUTHOR CONTRIBUTIONS

H.Z. and B.Z. conceived the study, designed the study, performed experiments and analyzed the data. H.Z., W.P., X.T., X.H., Lingjuan He, Q.L., Y.L., L.Z., Liang He and K.L. bred the mice and performed experiments. A.G. provided valuable comments, analyzed the data and edited the manuscript. B.Z. supervised the study, analyzed the data and wrote the manuscript.

COMPETING FINANCIAL INTERESTS

The authors declare no competing financial interests.

1. Ding, B.S. *et al.* Inductive angiocrine signals from sinusoidal endothelium are required for liver regeneration. *Nature* **468**, 310–315 (2010).
2. Malhi, H. & Gores, G.J. Cellular and molecular mechanisms of liver injury. *Gastroenterology* **134**, 1641–1654 (2008).
3. Ding, B.S. *et al.* Divergent angiocrine signals from vascular niche balance liver regeneration and fibrosis. *Nature* **505**, 97–102 (2014).
4. Wang, L. *et al.* Liver sinusoidal endothelial cell progenitor cells promote liver regeneration in rats. *J. Clin. Invest.* **122**, 1567–1573 (2012).
5. Matsumoto, K., Yoshitomi, H., Rossant, J. & Zaret, K.S. Liver organogenesis promoted by endothelial cells prior to vascular function. *Science* **294**, 559–563 (2001).
6. Lammert, E., Cleaver, O. & Melton, D. Induction of pancreatic differentiation by signals from blood vessels. *Science* **294**, 564–567 (2001).
7. Lammert, E., Cleaver, O. & Melton, D. Role of endothelial cells in early pancreas and liver development. *Mech. Dev.* **120**, 59–64 (2003).
8. Khan, J.A. *et al.* Fetal liver hematopoietic stem cell niches associate with portal vessels. *Science* **351**, 176–180 (2016).
9. Katz, T.C. *et al.* Distinct compartments of the proepicardial organ give rise to coronary vascular endothelial cells. *Dev. Cell* **22**, 639–650 (2012).
10. Red-Horse, K., Ueno, H., Weissman, I.L. & Krasnow, M.A. Coronary arteries form by developmental reprogramming of venous cells. *Nature* **464**, 549–553 (2010).
11. Wu, B. *et al.* Endocardial cells form the coronary arteries by angiogenesis through myocardial-endocardial VEGF signaling. *Cell* **151**, 1083–1096 (2012).
12. Tian, X. *et al.* Vessel formation. *De novo* formation of a distinct coronary vascular population in neonatal heart. *Science* **345**, 90–94 (2014).
13. Riley, P. Developmental biology: plumbing the heart. *Nature* **464**, 498–499 (2010).
14. Tian, X., Pu, W.T. & Zhou, B. Cellular origin and developmental program of coronary angiogenesis. *Circ. Res.* **116**, 515–530 (2015).
15. Buckingham, M., Meilhac, S. & Zaffran, S. Building the mammalian heart from two sources of myocardial cells. *Nat. Rev. Genet.* **6**, 826–835 (2005).
16. Ranger, A.M. *et al.* The transcription factor NF-ATc is essential for cardiac valve formation. *Nature* **392**, 186–190 (1998).
17. de la Pompa, J.L. *et al.* Role of the NF-ATc transcription factor in morphogenesis of cardiac valves and septum. *Nature* **392**, 182–186 (1998).
18. Chang, C.P. *et al.* A field of myocardial-endocardial NFAT signaling underlies heart valve morphogenesis. *Cell* **118**, 649–663 (2004).
19. Orkin, S.H. & Zon, L.I. Hematopoiesis: an evolving paradigm for stem cell biology. *Cell* **132**, 631–644 (2008).
20. Ginhoux, F. *et al.* Fate mapping analysis reveals that adult microglia derive from primitive macrophages. *Science* **330**, 841–845 (2010).
21. Zhang, H. *et al.* Endocardium contributes to cardiac fat. *Circ. Res.* **118**, 254–265 (2016).
22. Sauer, B. & McDermott, J. DNA recombination with a heterospecific Cre homolog identified from comparison of the pac-c1 regions of P1-related phages. *Nucleic Acids Res.* **32**, 6086–6095 (2004).
23. Anastassiadis, K. *et al.* Dre recombinase, like Cre, is a highly efficient site-specific recombinase in *E. coli*, mammalian cells and mice. *Dis. Model. Mech.* **2**, 508–515 (2009).
24. Madisen, L. *et al.* Transgenic mice for intersectional targeting of neural sensors and effectors with high specificity and performance. *Neuron* **85**, 942–958 (2015).
25. Tian, X. *et al.* Subepicardial endothelial cells invade the embryonic ventricle wall to form coronary arteries. *Cell Res.* **23**, 1075–1090 (2013).
26. Breier, G., Albrecht, U., Sterrer, S. & Risau, W. Expression of vascular endothelial growth factor during embryonic angiogenesis and endothelial cell differentiation. *Development* **114**, 521–532 (1992).
27. Nagy, J.A., Dvorak, A.M. & Dvorak, H.F. VEGF-A and the induction of pathological angiogenesis. *Annu. Rev. Pathol.* **2**, 251–275 (2007).
28. Carmeliet, P. & Jain, R.K. Molecular mechanisms and clinical applications of angiogenesis. *Nature* **473**, 298–307 (2011).
29. Shalaby, F. *et al.* Failure of blood-island formation and vasculogenesis in Flk-1–deficient mice. *Nature* **376**, 62–66 (1995).
30. Carmeliet, P. Blood vessels and nerves: common signals, pathways and diseases. *Nat. Rev. Genet.* **4**, 710–720 (2003).
31. Haigh, J.J. *et al.* Cortical and retinal defects caused by dosage-dependent reductions in VEGF-A paracrine signaling. *Dev. Biol.* **262**, 225–241 (2003).
32. Goldman, O. *et al.* Endoderm generates endothelial cells during liver development. *Stem Cell Rep.* **3**, 556–565 (2014).

ONLINE METHODS

Experimental mice. All mouse studies were carried out in strict accordance with the guidelines of the Institutional Animal Care and Use Committee (IACUC) at the Institute for Nutritional Sciences, Shanghai Institutes for Biological Sciences, Chinese Academy of Sciences. The morning of vaginal plug detection was designated as E0.5. 4-Hydroxytamoxifen (4-OHT; Sigma) was dissolved in ethanol and corn oil at a 1:4 ratio. Tamoxifen was introduced by oral gavage at the indicated times (0.15–0.2 mg/g). *Rosa26-RFP*, Ai66 (*Rosa26*-RSR-LSL-*RFP*) and $Kdr^{fl/fl}$ mice were reported previously[24,31,33]. The *Rosa26*-RSR-*RFP* mouse line was generated by crossing *Actb-cre* mice[34] with Ai66 mice to excise the *loxP*-flanked stop cassette, and *Actb-cre* was not passaged to the subsequent generation. The *Nfatc1-dre* mouse line was generated by genome editing using CRISPR/Cas9 (ref. 21). A cDNA encoding the Dre recombinase followed by a polyadenylation sequence was inserted into the last exon of *Nfatc1*, and a 2A peptide sequence was included before the cDNA to link the *Nfatc1* coding region and *dre*. The *Nfatc1*-IRES-*creER* line was generated by genome editing using CRISPR/Cas9. A cDNA encoding Cre recombinase fused with a mutant form of the estrogen receptor hormone-binding domain C ($CreER^{T2}$) followed by an IRES was introduced into the XhoI site in the *Nfatc1* 3′UTR. The *Nfatc1-GFP* line was generated by genome editing using CRISPR/Cas9. A cDNA encoding a GFP-Cre fusion protein was inserted into the last common coding exon of *Nfatc1*, and a 2A peptide sequence was included to link *Nfatc1* and *GFP-cre* to allow expression of both genes. *Npr3-creER* was generated by conventional homologous recombination in embryonic stem (ES) cells and blastocyst injection of correctly targeted ES cell clones. A cDNA encoding $CreER^{T2}$ was inserted in frame with the translational start codon of the *Npr3* gene. Chimeric mice positive for targeted ES cells were germline transferred to the F_1 generation and bred on a C57BL/6; ICR background. The *Nfatc1-dre*, *Nfatc1-GFP* and *Npr3-creER* lines were generated by Shanghai Biomodel Organism Co., Ltd, and the *Nfatc1*-IRES-*creER* line was generated by Shanghai Yaobang Biotechnology Co., Ltd. All experimental mice were maintained on a C57BL/6; ICR background.

Genomic PCR. Genomic DNA was prepared from embryonic yolk sac or mouse tail. Tissues were lysed by incubation with proteinase K overnight at 55 °C, followed by centrifugation at maximum speed (21,130*g*) for 5 min to obtain supernatant with genomic DNA. DNA was precipitated by adding isopropanol and was washed in 70% ethanol. All embryos and mice were genotyped with specific primers that distinguished the knock-in allele from the wild-type allele. The genotyping primers are listed in **Supplementary Table 1**.

Whole-mount immunohistochemistry and immunofluorescence. Whole-mount immunostaining was performed according to previously described methods[35]. Embryos from timed pregnancies were collected in PBS and fixed in 4% paraformaldehyde (PFA) overnight at 4 °C. After three washes with cold PBS for 10 min each, embryos were left intact in 1.5-ml tubes and stored in 70% ethanol at 4 °C for a few days. Embryos were dehydrated through a methanol gradient (25%, 50%, 75% and 100% methanol in PBS) for 15 min at each step at room temperature. After dehydration, embryos were incubated with 6% hydrogen peroxide diluted in methanol for 2 h at 4 °C with constant rotation. Embryos were serially rehydrated in 100%, 75%, 50% and 25% methanol in PBS for 15 min at each step at room temperature. After washing in PBS with 0.1% Tween-20 for 10 min, embryos were incubated in blocking solution (5% donkey serum and 0.1% Triton X-100 in PBS) for 1 h at 4 °C or room temperature. Primary antibodies in blocking solution were incubated with embryos overnight at 4 °C with constant rotation, followed by washes with PBT (PBS with 0.1% Triton X-100) for 4 h at 4 °C. Embryos were left in PBT overnight at 4 °C with constant rotation. Primary antibodies were used as listed: ESR (Abcam, ab27595; prediluted or 1:1 dilution), NKX2-5 (Santa Cruz Biotechnology, sc-8697; 1:100 dilution) and TNNI3 (Abcam, ab56357; 1:100 dilution). Secondary antibodies were incubated with embryos for 2 h at room temperature, followed by PBT washes for 4 h. Secondary antibodies were used as listed: Immpress anti-rabbit immunoglobulin (Vector, MP-7401-50; prediluted or 1:1 dilution), donkey anti-goat 488 (Invitrogen, A11055; 1:250 dilution) and donkey anti-goat 555 (Invitrogen, A21432; 1:250 dilution). For whole-mount immunohistochemistry, the ImmPACT DAB kit (Vector, sk-4150; 10 µl of DAB in 1 ml of dilution buffer) was used to develop the color to the desired extent. Images were acquired on a Leica stereomicroscope (M165FC).

Immunofluorescent staining on cryosections. Immunostaining was performed according to previously described protocols[36]. Briefly, embryos, hearts or livers were collected in PBS and washed to remove excessive blood. Embryos or tissues were then fixed in 4% PFA for 15–30 min. After three washes in PBS, embryos or tissues with fluorescence reporters were observed and photographed using fluorescence microscopy (Leica M165FC or Zeiss AXIO Zoom V16). Then, embryos or tissues were dehydrated in 30% sucrose in PBS and embedded in OCT (Sakura). For embryos at E8.0–E8.5, cryosections of 7–8 µm in thickness were collected. For late-stage embryos or adult livers, cryosections of 8–10 µm in thickness were collected. After air drying for 1 h at room temperature, sections were blocked with blocking buffer (5% donkey serum and 0.1% Triton X-100 in PBS) for 30 min at room temperature, followed by incubation with primary antibody at 4 °C overnight. The following antibodies were used: NKX2-5 (Santa Cruz Biotechnology, sc-8697; 1:100 dilution), TNNI3 (Abcam, ab56357; 1:100 dilution), ESR (Abcam, ab27595; prediluted or 1:1 dilution), PECAM1 (BD, 553370; 1:500 dilution), RFP (ChromoTek, ABIN334653; 1:200 dilution), RFP (Rockland, 600-401-379; 1:1,000 dilution), FOXA2 (Santa Cruz Biotechnology, sc-6554; 1:100 dilution), VE-cadherin (R&D, AF1002; 1:100 dilution), HNF4A (Abcam, ab41898; 1:200 dilution), HNF4A (Santa Cruz Biotechnology, sc-6556; 1:200 dilution), GFP (Invitrogen, A21311; 1:100 dilution), DESMIN (R&D, AF3844; 1:100 dilution), SMA-FITC (Sigma, F3777; 1:400 dilution), CK19 (Developmental Studies Hybridoma Bank, TROMA-III; 1:500 dilution), EPCAM (Abcam, ab92382; 1:1,000 dilution), PDGFRA (R&D, AF1062; 1:500 dilution), ENG (BD, 550546; 1:50 dilution), LYVE1 (Abcam, ab14917; 1:100 dilution), PROX1 (R&D, AF2727; 1:500 dilution), Ephb4 (R&D, AF446; 1:100 dilution), VEGFR2 (BD, 550549; 1:50 dilution), NFATC1 (Santa Cruz Biotechnology, sc-7294; 1:100 dilution), Ki-67 (Lab Vision, RM-9106-F1; 1:100 dilution), PHH3 (Upstate, 06-570; 1:1,000 dilution) and PCNA (Cell Signaling Technology, 13110; 1:500 dilution). Signals were developed with fluorescence-conjugated antibodies (Invitrogen) used at a dilution of 1:1,000 for 30 min at room temperature. For ESR and PECAM1 staining, we combined horseradish peroxidase (HRP)-conjugated antibodies (Vector) with the tyramide signal amplification kit (PerkinElmer) to develop the color. After three washes in PBS, sections were counterstained with DAPI (Vector Lab). Images were acquired on a Zeiss (LSM510) or Olympus (FV1000) confocal microscope.

***In situ* hybridization.** *In situ* hybridization was performed as previously described[37]. Briefly, embryos were collected in DEPC-treated PBS and fixed overnight in 4% fresh PFA. After three washes in PBS, embryos were dehydrated in 30% sucrose, which was also dissolved in DEPC-treated PBS. Then, embryos were embedded in OCT and could be stored at −80 °C after they were frozen. Cryosections of 8–10 µm in thickness were collected. After air drying for 1 h at room temperature, slides were incubated with antisense probes (1 µg/ml) overnight at 65 °C. After two washes in MABT buffer (pH 7.5) for 5 min each, slides were washed in SSC buffer containing 50% formamide for 70 min at 65 °C. Then, slides were equilibrated in MABT buffer for 15 min and blocked in blocking buffer (10% sheep serum and 2% blocking reagent in MABT buffer) for 1 h or longer at room temperature. Alkaline phosphatase–coupled antibody to digoxigenin was incubated with sections for 2 h at room temperature at a dilution of 1:2,000. After washing in MABT buffer and equilibration in NTMT buffer, sections were developed with BCIP/NBT (Promega, S3771) in the dark to the desired extent. Slides were mounted in glycerol. Images were acquired on an Olympus microscope (BX53). The primers used to generate the *Npr3* and *Vegfa* probes are listed in **Supplementary Table 1**.

Statistical analysis. All data were determined from 3–5 independent experiments as indicated in each figure legend and are presented as mean values ± s.e.m. All mice were randomly assigned to different experimental groups. No statistical method was used to predetermine sample size.

doi:10.1038/ng.3536

33. Madisen, L. *et al.* A robust and high-throughput Cre reporting and characterization system for the whole mouse brain. *Nat. Neurosci.* **13**, 133–140 (2010).
34. Lewandoski, M., Meyers, E.N. & Martin, G.R. Analysis of *Fgf8* gene function in vertebrate development. *Cold Spring Harb. Symp. Quant. Biol.* **62**, 159–168 (1997).
35. He, L. *et al.* BAF200 is required for heart morphogenesis and coronary artery development. *PLoS One* **9**, e109493 (2014).
36. Zhou, B. *et al.* Adult mouse epicardium modulates myocardial injury by secreting paracrine factors. *J. Clin. Invest.* **121**, 1894–1904 (2011).
37. Zhang, H. *et al.* Yap1 is required for endothelial to mesenchymal transition of the atrioventricular cushion. *J. Biol. Chem.* **289**, 18681–18692 (2014).